Eur. Phys. J. Special Topics **228**, 1839–1854 (2019)

https://doi.org/10.1140/epjst/e2019-800241-y

THE EUROPEAN PHYSICAL JOURNAL SPECIAL TOPICS

Regular Article

Frequency-amplitude characteristics of periodic motions in a periodically forced van der Pol oscillator

Yeyin Xu and Albert C.J. Luo[a]

Department of Mechanical and Industrial Engineering, Southern Illinois University Edwardsville, Edwardsville, IL 62026-1805, USA

Received 30 December 2018 / Received in final form 3 July 2019
Published online 25 September 2019

Abstract. In this paper, nonlinear frequency-amplitude characteristics of periodic motions in a periodically forced van der Pol oscillator are studied systematically. The periodic motions of the van der Pol oscillator are determined by the semi-analytical method, and the corresponding stability and bifurcation analysis is completed through the eigenvalue analysis. From the finite Fourier series analysis, the nonlinear frequency-amplitude characteristics of periodic motions are analyzed. From the frequency-amplitude analysis, the limit cycle of the van der Pol oscillator can be obtained analytically as excitation amplitude approach to zero, rather than numerically. For the van der Pol oscillator, most of periodic motions in the van der pol oscillator are symmetric. However, an asymmetric period-1 motion in the van der Pol oscillator is discovered. Thus a bifurcation tree of period-1 motion to chaos can be found.

1 Introduction

Dynamical systems experiencing the fast-slow motions extensively exist in engineering and science. The fast-slow periodic motions in such dynamical systems cannot be easily solved by the traditional analysis because such fast-slow periodic motions need many harmonic terms to get appropriate approximate solutions. The fast movement is like an impulsive motion, and the slow movement is like almost zero velocity movement. The semi-analytical method can achieve very higher order harmonics in periodic motions. Further, the fast-slow movements of periodic motions in such nonlinear systems can be caught. Therefore, in this paper, the semi-analytical method will be used to obtain periodic motions with such fast-slow varying movements in such nonlinear dynamical systems. The van der Pol oscillator is a typical oscillator possessing the fast-slow motions. Through studies on the van der Pol oscillator, the fast-slow movements of periodic motions in nonlinear dynamical systems will be better understood.

In 1920, van der Pol [1] determined periodic motions of self-excited circuit systems through the method of averaging. In 1923, Greaves [2] studied the analytical solutions of the van der Pol oscillator and found a family of periodic solutions. In 1927,

[a] e-mail: aluo@siue.edu

van der Pol and van der Mark [3] discovered the van der Pol system was capable of oscillating with the discrete frequencies and there was irregular noise in the process when one frequency jumps to the next low value. In 1934, van der Pol [4] studied the resonant curves in the forced van der Pol oscillators. He found the resonant curves had usual shapes for a strong signal, while for a relatively weak signal, the curves could be warped. In 1945, Cartwright and Littlewood [5] proved the existence of periodic solutions of the van der Pol equation. In 1947, Cartwright and Littlewood [6] studied the periodic solutions of a generalized nonlinear equation based on the van der Pol and Duffing equations. The periodic solutions of the Duffing equation were discussed. However, the solutions of the van der Pol equation were discussed in Littlewood [7]. In 1948, Levinson [8] used three piecewise linear differential equations to model the van der Pol equation and proved the existence of periodic solutions. In 1949, Levinson [9] further used the piecewise linear model of the van der Pol equation and discovered the countable infinite periodic sequences in such a second order differential equation. In 1982, Andersen and Geer [10] computed the frequency and period of the limit cycle of the van der Pol equation through perturbation analysis. In 1984, Dadfar, Geer and Andersen [11] used the perturbation analysis to further investigate periodic motions in a van der Pol equation. In 1998, Buonomo [12] also used the perturbation analysis to determine the limit cycle of the van der Pol equation. Buonomo [13] studied the periodic solutions of the van der Pol equation through the combination of the perturbation method and harmonic balance method. In 2002, Mickens [14] studied a van der Pol equation through the backward Euler method. Mickens [15] applied the modified harmonic balance method to the van der Pol system. In 2006, Waluya and van Horssen [16] used the variables of energy and phase angle to present asymptotical solutions of periodic motions. Andrianov and van Horssen [17] applied the same method to a generalized van der Pol equation, and the approximate periodic solutions of the van der Pol equations were based on the the perturbed linear system with small parameters. In addition, one used the perturbation methods to investigate periodic motions and chaos in nonlinear systems recently. In 2016, Maaita [18] studied the bifurcation of the slow invariant manifold of two linear oscillators coupled to a k-order nonlinear oscillator. In 2017, Yamgoue et al. [19] studied the approximate analytical solutions of a constrained nonlinear mechanical system. Shayak and Vyas [20] studied the Mathieu equation by using the Krylov-Bogoliubov method. Rajamani and Rajasekar [21] used the perturbation method for the response amplitude of the parametric Duffing oscillator. The aforementioned methods include the perturbation methods and the classic harmonic balance method. From the existing studies, the perturbation methods require the corresponding linear solutions for the approximate periodic solutions of the original nonlinear systems, and the perturbation expansion with small parameters was adopted, which is not adequate.

To resolve the abovementioned puzzles in nonlinear dynamical systems, in 2012, Luo [22] developed a generalized harmonic balance method based on the finite Fourier series. The generalized harmonic balance method gives analytical solutions of periodic motions, and the corresponding bifurcations and stability of periodic motions can be determined. In 2012, Luo and Huang [23] applied the generalized harmonic balance method for the stable and unstable period-m motions of a Duffing oscillator with a nonlinear damping. The analytical routes of period-1 motion to chaos in a Duffing oscillator were studied in Luo and Huang [24] through the generalized harmonic balance method. In 2013, Luo and Lakeh [25] applied the generalized harmonic balance method to a periodically forced van der Pol oscillator, and the analytical solutions of period-1, period-3 and period-5 motions were obtained. In 2014, Luo and Lakeh [26] studied a van der Pol-Duffing oscillator through the generalized harmonic balance method, and the corresponding bifurcation trees of periodic motions to chaos were obtained.

The generalized harmonic balance method is very good for the polynomial nonlinear systems, However, it is very difficult to apply such a method to non-polynomial nonlinear systems. Thus, in 2015, Luo [27,28] developed the semi-analytical method through implicit mappings. The implicit mappings were obtained from the discretization of nonlinear dynamic systems. In 2015, Luo and Guo [29] investigated a Duffing oscillator by the semi-analytical method, and the bifurcation trees of periodic motions were predicted analytically. Guo and Luo [30] used such a method to obtain the route of periodic motions to chaos in a periodically forced pendulum dynamic system. In 2016, Luo and Xing [31] studied the period-1 motions to chaos in a periodically forced, time-delayed, hardening Duffing oscillator. In 2017, Luo and Xing [32] studied the bifurcation trees of period-3 motions to chaos in a time-delayed hardening Duffing oscillator. In 2018, Xu and Luo [33] presented the periodic motions in van der Pol-Duffing oscillator through the semi-analytical method. In Xu and Luo [34], found was the van der Pol oscillator possessed a sequential period-$(2m-1)$ motions to chaos as

$$P_1 \lhd P_3 \lhd \cdots \lhd P_{2m-1} \lhd P_{2m+1} \cdots \lhd \text{Chaos}.$$

In such a sequence, the period-$(2m-1)$ motions exist in specific frequency ranges. Such a property of periodic motions can be used for control different periodic motions in specific frequency ranges. However, it is also important that the frequency-amplitude characteristics of periodic motions vary with excitation amplitudes. Thus, the semi-analytical method will be used herein to study frequency-amplitude characteristics of periodic motions in the von der Pol oscillator.

In this paper, periodic motions of a periodically forced van der Pol oscillator will be studied through the semi-analytical method, and the harmonic frequency-amplitude characteristics of periodic motion will be presented through the discrete Fourier analysis for prescribed excitation amplitudes. The stability and bifurcation of periodic motions will be determined through eigenvalue analysis. As excitation amplitude approaches zero, the stable or unstable limit cycle will be determined. Numerical simulation will be completed for the comparison of numerical and analytical results.

2 Discretization

Consider a van der Pol oscillator as

$$\ddot{x} + (-\alpha_1 + \alpha_2 x^2)\dot{x} + \beta x = Q_0 \cos \Omega t \tag{1}$$

where α_1 and α_2 represent linear and nonlinear damping coefficients, respectively. β represents the linear stiffness coefficient. Q_0 and Ω are excitation amplitude and frequency, respectively. In phase space, equation (1) becomes

$$\begin{aligned} \dot{x} &= y, \\ \dot{y} &= -(-\alpha_1 + \alpha_2 x^2)\dot{x} - \beta x + Q_0 \cos \Omega t. \end{aligned} \tag{2}$$

As in Luo [24,27,28], for $t \in [t_{k-1}, t_k]$, the van der Pol oscillator can be discretized by a midpoint scheme and forms a mapping P_k $(k \in \{1, 2, 3, \ldots\})$

$$P_k : \mathbf{x}_{k-1} \to \mathbf{x}_k \Rightarrow \mathbf{x}_k = P_k \mathbf{x}_{k-1} \tag{3}$$

where $\mathbf{x}_k = (x_k, y_k)^{\mathrm{T}}$ is a discrete node of motion in phase space. The mapping P_k $(k \in \{1, 2, \ldots\})$ is

$$
\begin{aligned}
x_k &= x_{k-1} + \tfrac{1}{2}h(y_k + y_{k-1}),\\
y_k &= y_{k-1} + h\{\tfrac{1}{8}[4\alpha_1 - \alpha_2(x_k + x_{k-1})^2](y_k + y_{k-1}) - \tfrac{1}{2}\beta(x_k + x_{k-1})\\
&\quad + Q_0 \cos\Omega(t_{k-1} + \tfrac{1}{2}h)\}.
\end{aligned} \tag{4}
$$

where $h = t_k - t_{k-1}$ is time step.

For a periodic motion, there is a mapping structure with $(N+1)$ nodes as

$$
P = P_N \circ P_{N-1} \circ \cdots \circ P_1 : \mathbf{x}_0 \to \mathbf{x}_N. \tag{5}
$$

Thus

$$
\mathbf{x}_N = P\mathbf{x}_0 = P_N \circ P_{N-1} \circ \cdots \circ P_1\mathbf{x}_0. \tag{6}
$$

That is,

$$
\mathbf{x}_N = P_N\mathbf{x}_{N-1},\ \mathbf{x}_{N-1} = P_{N-1}\mathbf{x}_{N-2},\ \ \ldots,\ \mathbf{x}_1 = P_1\mathbf{x}_0. \tag{7}
$$

The corresponding algebraic equations for mapping P_k $(k = 1, 2, \ldots, N)$ is given by $\mathbf{g}(\mathbf{x}_{k-1}, \mathbf{x}_k) = \mathbf{0}$ with $\mathbf{g}_k = (g_{1,k}, g_{2,k})^{\mathrm{T}}$, i.e.,

$$
\begin{aligned}
g_{1,k} &= x_k - x_{k-1} - \tfrac{1}{2}h(y_k + y_{k-1}) = 0,\\
g_{2,k} &= y_k - y_{k-1} + h\{\tfrac{1}{8}[-4\alpha_1 + \alpha_2(x_k + x_{k-1})^2](y_k + y_{k-1})\\
&\quad + \tfrac{1}{2}\beta(x_k + x_{k-1}) - Q_0 \cos\Omega(t_{k-1} + \tfrac{1}{2}h)\}\\
&= 0,
\end{aligned} \tag{8}
$$

and the periodicity condition requires

$$
(x_N, y_N)^{\mathrm{T}} = (x_0, y_0)^{\mathrm{T}}. \tag{9}
$$

Equations (8) and (9) possess $2(N+1)$ equations for $2(N+1)$ unknowns. Once the discrete nodes are obtained, the stability and bifurcations of periodic motions in the van der Pol oscillator can be determined through eigenvalue analysis. Consider a small variation $\Delta\mathbf{x}_k$ in the vicinity of $\mathbf{x}_k^*$ (i.e., $\mathbf{x}_k = \mathbf{x}_k^* + \Delta\mathbf{x}_k$, $k = 1, 2, \ldots, N$), the linearized equation of the implicit mapping structure is

$$
\frac{\partial \mathbf{g}_k}{\partial \mathbf{x}_{k-1}}\Big|_{(\mathbf{x}_{k-1}^*, \mathbf{x}_k^*)}\Delta\mathbf{x}_{k-1} + \frac{\partial \mathbf{g}_k}{\partial \mathbf{x}_k}\Big|_{(\mathbf{x}_{k-1}^*, \mathbf{x}_k^*)}\Delta\mathbf{x}_k = \mathbf{0}. \tag{10}
$$

Deformation of equation (10) gives

$$
\Delta\mathbf{x}_k = DP_k\Delta\mathbf{x}_{k-1} = -\left[\frac{\partial \mathbf{g}_k}{\partial \mathbf{x}_k}\right]^{-1}\left[\frac{\partial \mathbf{g}_k}{\partial \mathbf{x}_{k-1}}\right]_{(\mathbf{x}_{k-1}^*, \mathbf{x}_k^*)}\Delta\mathbf{x}_{k-1} \tag{11}
$$

where

$$
DP_k = \left[\frac{\partial \mathbf{x}_k}{\partial \mathbf{x}_{k-1}}\right]_{(\mathbf{x}_k^*, \mathbf{x}_{k-1}^*)} = \begin{bmatrix} \frac{\partial x_k}{\partial x_{k-1}} & \frac{\partial x_k}{\partial y_{k-1}} \\ \frac{\partial y_k}{\partial x_{k-1}} & \frac{\partial y_k}{\partial y_{k-1}} \end{bmatrix}_{(\mathbf{x}_{k-1}^*, \mathbf{x}_k^*)} \tag{12}
$$

with

$$\begin{aligned}
\frac{\partial x_k}{\partial x_{k-1}} &= \frac{8-h^2(\alpha_2\Delta_1-2\beta+4h\beta)+\Delta_2}{8+h^2\alpha_2\Delta_1+2h^2\beta+\Delta_2},\\
\frac{\partial x_k}{\partial y_{k-1}} &= \frac{\left[(16+\Delta_2)-(2\beta-\Delta_2)\,h^2\right]h}{2(8+h^2\alpha_2\Delta_1+2h^2\beta+\Delta_2)},\\
\frac{\partial y_k}{\partial x_{k-1}} &= -\frac{4h(\alpha_2\Delta_1+2h\beta)}{8+h^2\alpha_2\Delta_1+2h^2\beta+\Delta_2},\\
\frac{\partial y_k}{\partial y_{k-1}} &= \frac{8-h^2\left(\alpha_2\Delta_1+4\beta-\Delta_2\right)}{8+h^2\alpha_2\Delta_1+2h^2\beta+\Delta_2},\\
\Delta_1 &= (x_k+x_{k-1})\,(y_k+y_{k-1}),\\
\Delta_2 &= -4\alpha_1+\alpha_2\,(x_k+x_{k-1})^2.
\end{aligned} \tag{13}$$

From the mapping structure, the perturbed variation of Δx_N is

$$\Delta\mathbf{x}_N = DP\Delta\mathbf{x}_0 = \underbrace{DP_N\cdot DP_{N-1}\cdot\ldots\cdot DP_2\cdot DP_1}_{N-\text{multiplication}}\Delta\mathbf{x}_0. \tag{14}$$

The resultant Jacobian matrix of the periodic motion is

$$\begin{aligned}
DP &= \left[\frac{\partial\mathbf{x}_N}{\partial\mathbf{x}_0}\right]_{(\mathbf{x}_N^*,\mathbf{x}_{N-1}^*,\ldots,\mathbf{x}_0^*,)} = DP_N\cdot DP_{N-1}\cdot\ldots\cdot DP_2\cdot DP_1\\
&= \prod_{k=N}^{1}\left[\frac{\partial\mathbf{x}_k}{\partial\mathbf{x}_{k-1}}\right]_{(\mathbf{x}_k^*,\mathbf{x}_{k-1}^*)}.
\end{aligned} \tag{15}$$

The stability and bifurcation of period-1 motion is determined by

$$|DP-\lambda\mathbf{I}_{2\times2}| = 0. \tag{16}$$

From Luo [27,28], the stability of such a periodic motion is determined as follows.

i. If the magnitudes of all eigenvalues of DP are less than one (i.e. $|\lambda_i|<1$, $i=1,2$), the periodic solution is stable.
ii. If the magnitude of at least one eigenvalue of DP is greater than one (i.e. $|\lambda_i|>1$, $i\in\{1,2\}$), the periodic solution is unstable.
iii. The boundaries between stable and unstable periodic motion with higher order singularity can generate bifurcation and stability conditions with higher order singularity.

The bifurcation conditions are given as follows.

i. If $\lambda_i=1$ with $|\lambda_j|<1$ $(i,j\in\{1,2\}, i\neq j)$, the saddle-node bifurcation (SN) occurs.
ii. If $\lambda_i=-1$ with $|\lambda_j|<1$ $(i,j\in\{1,2\}, i\neq j)$, the period-doubling bifurcation (PD) occurs.
iii. If $|\lambda_i|=|\lambda_j|=1$ $(i,j\in\{1,2\}, \lambda_i=\bar{\lambda}_j, i\neq j)$, the Neimark bifurcation (NB) occurs.

3 Semi-analytical solutions

The discrete implicit mapping in equation (3) has a computational accuracy of $\varepsilon = O(h^3)$. If $\varepsilon=10^{-9}$, the time step should be $h\le 10^{-3}$. Because $h=\Delta t=T/N$, we have $N=T/h=2\pi/\Omega h$. Consider a set of parameters as

$$\alpha_1=16,\ \alpha_2=1,\ \beta=5. \tag{17}$$

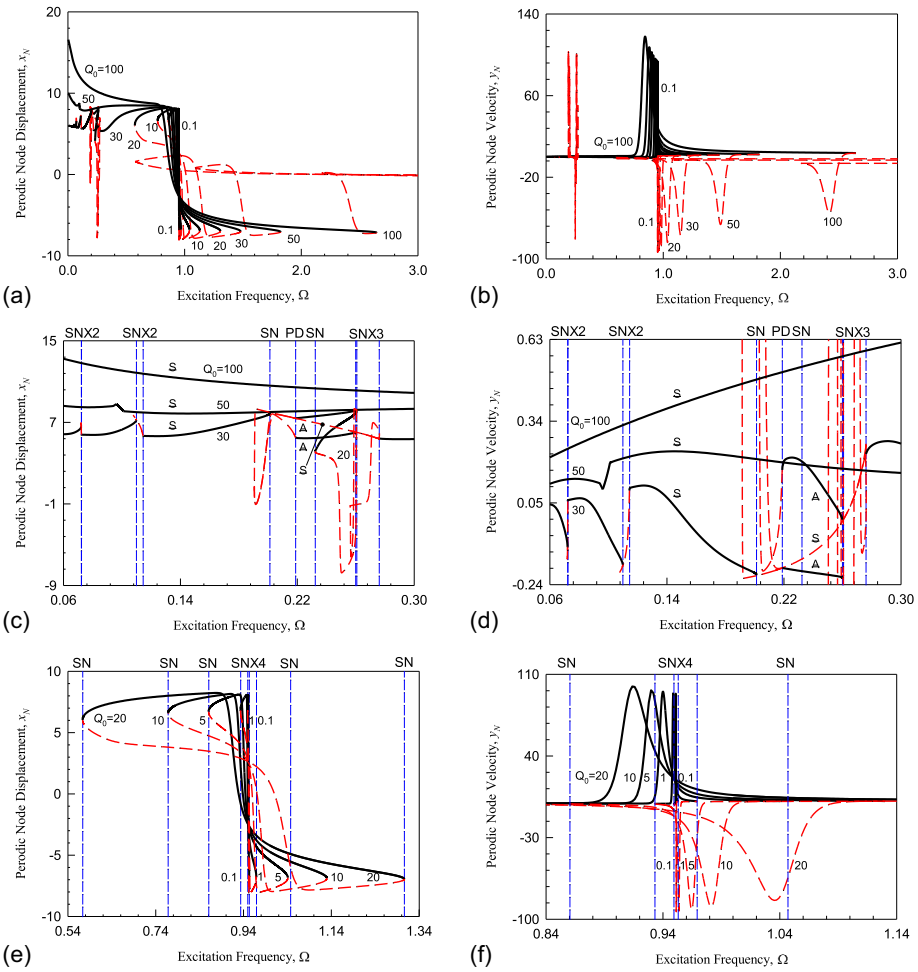

Fig. 1. Period-1 motions varying with excitation frequency ($\Omega \in (0, 3.0)$). Global view: (a) displacement x_N, (b) velocity y_N. Zoomed view-I ($\Omega \in (0.06, 0.3)$): (c) displacement x_N, (d) velocity y_N. Zoomed view-II: (e) displacement x_N ($\Omega \in (0.54, 1.34)$), (f) velocity y_N ($\Omega \in (0.84, 1.147)$). ($\alpha_1 = 16, \alpha_2 = 1, \beta = 5$).

The discrete nodes (x_N, y_N) of period-1 motions varying with excitation frequency are presented in Figure 1. Solid and dashed curves represent stable and unstable solutions of period-1 motions, respectively. The acronym "SN" is for saddle-node bifurcation. In Figures 1a and 1b, periodic node displacement x_N and velocity y_N of the period-1 motions are presented, respectively. For low frequency, the first zoomed views of displacement x_N and velocity y_N are presented in Figures 1c and 1d for $Q_0 = 30, 50, 100$. The second zoomed views of displacement x_N and velocity y_N are presented in Figures 1e and 1f for $Q_0 = 0.1, 1, 5, 10, 20$. If $Q_0 = 0$, the limit cycle for the van der Pol oscillator is obtained.

The period-1 motion for $Q_0 = 100$ is stable for $\Omega \in (0, 2.645)$ and unstable for $\Omega \in (2.193, 2.645)$ and $(2.193, \infty)$. A saddle-node bifurcation occurs at $\Omega_{cr} \approx 2.645$ for jumping. For $Q_0 = 50$, the period-1 motion is stable for $\Omega \in (0, 1.823)$ and unstable for $\Omega \in (1.105, 1.823)$ and $(1.105, \infty)$. A saddle-node bifurcation occurs at $\Omega_{cr} \approx 1.823$. For $Q_0 = 30, 50, 100$, the period-1 motions exist for $\Omega \in (0, \infty)$. With excitation amplitude becoming smaller, period-1 motions exist in vicinity of the limit

Table 1. Frequency ranges of stable periodic motions for different excitation amplitudes ($\alpha_1 = 16, \alpha_2 = 1, \beta = 5, \Omega \in (0, 3)$.

Q_0	Ω	SN(L)	SN(R)
100	(0, 2.645)	–	2.645
50	(0, 1.823)	–	1.823
30.0	(0.0721, 0.0722)	0.0721	0.0722
	(0.110, 0.114)	0.110	0.114
	(0.201, 0.276)	0.201	0.276
	(0.219, 0.260)	0.219(PD)	0.260
	(0.260, 0.276)	0.260	0.276
	(–,1.480)	–	1.480
20.0	(0.573, 1.306)	0.573	1.306
	(0.232, 0.261)	0.232	0.261
10.0	(0.768, 1.130)	0.768	1.130
5.0	(0.860, 1.041)	0.860	1.041
1.0	(0.933, 0.969)	0.933	0.969
0.1	(0.949, 0.953)	0.949	0.953

cycle. For $Q_0 = 20$, the corresponding period-1 motion exists in $\Omega \in (0.573, 1.306)$. The two saddle-node bifurcations are at $\Omega_{\rm cr} \approx 0.573, 1.306$. The period-1 motion is a closed loop of stable and unstable. For $Q_0 = 10$, the stable and unstable period-1 motions exist in the range of $\Omega \in (0.768, 1.130)$. Two saddle-node bifurcations are at $\Omega_{\rm cr} \approx 0.768, 1.130$. The closed loop of stable and unstable period-1 motion becomes smaller. For $Q_0 = 5$, the closed loop of stable and unstable period-1 motions is in $\Omega \in (0.860, 1.040)$ with two saddle-node bifurcations of $\Omega_{\rm cr} = 0.860, 1.040$. For $Q_0 = 1$, a closed loop of unstable and stable period-1 motions occur in $\Omega \in (0.933, 0.969)$ with the saddle-node bifurcations of $\Omega_{\rm cr} = 0.933, 0.969$. For $Q_0 = 0.1$, the period-1 motions occur in $\Omega \in (0.949, 0.953)$ with two saddle-node bifurcations of $\Omega_{\rm cr} \approx 0.949, 0.952$. With decreasing the excitation amplitude, the frequency range of period-1 motions in the van der Pol oscillator will shrink to the frequency of the limit cycle. Thus, at $Q_0 = 0$, the limit cycle possesses a frequency $\Omega \in (0.949, 0.953)$. In Table 1, the frequency ranges of stable period-1 motions with different excitation amplitudes are tabulated.

4 Amplitude-frequency characteristics

Based on the semi-analytical results of discrete nodes, the corresponding periodic motions can be approximately expressed by a finite Fourier series as

$$\mathbf{x}(t) \approx \mathbf{a}_0 + \sum_{j=1}^{M} \mathbf{b}_j \cos(j\Omega t) + \mathbf{c}_j \sin(j\Omega t) \tag{18}$$

where $\mathbf{a}_0$, $\mathbf{b}_j$ and $\mathbf{c}_j$ $(j = 1, 2, \ldots, M)$ are unknown coefficients. Consider $M = N/2$, the analytical prediction $\mathbf{x}_k$ $(k = 1, 2, \ldots, N)$ for the period-1 motion is expressed with $t \in [0, T]$ as

$$\mathbf{x}(t_k) = \mathbf{x}_k \approx \mathbf{a}_0 + \sum_{j=1}^{N/2} \mathbf{b}_j \cos(j\Omega t_k) + \mathbf{c}_j \sin(j\Omega t_k)$$
$$\approx \mathbf{a}_0 + \sum_{j=1}^{N/2} \mathbf{b}_j \cos\left(\frac{2\pi kj}{N}\right) + \mathbf{c}_j \sin\left(\frac{2\pi kj}{N}\right) \tag{19}$$

where $\Delta t = T/N = 2\pi/(\Omega N), t_k = t_0 + k\Delta t = 2\pi k/(\Omega N)$ for $(t_0 = 0, k = 0, 1, \ldots, N)$. The coefficients of $\mathbf{a}_0$, $\mathbf{b}_j$ and $\mathbf{c}_j$ are determined by

$$\mathbf{a}_0 = \tfrac{1}{N}\sum_{k=0}^{N-1} \mathbf{x}_k,\ \mathbf{b}_j = \tfrac{2}{N}\sum_{k=0}^{N-1} \mathbf{x}_k \cos\left(\tfrac{2\pi kj}{N}\right),\ \mathbf{c}_j = \tfrac{2}{N}\sum_{k=0}^{N-1} \mathbf{x}_k \sin\left(\tfrac{2\pi kj}{N}\right),$$
$$(j = 1, 2, \ldots, N/2). \tag{20}$$

Since $\mathbf{x}_k = (x_k, y_k)^{\mathrm{T}}$ $(k = 1, 2, \ldots, N)$, for the coefficients, they have:

$$\mathbf{a}_0 = (a_{1,0}, a_{1,0})^{\mathrm{T}}, \mathbf{b}_j = (b_{1,j}, b_{2,j})^{\mathrm{T}}, \mathbf{c}_j = (c_{1,j}, c_{2,j})^{\mathrm{T}}. \tag{21}$$

Thus equation (18) becomes

$$\left\{ \begin{array}{c} x(t) \\ y(t) \end{array} \right\} \approx \left\{ \begin{array}{c} a_{1,0} \\ a_{2,0} \end{array} \right\} + \sum_{j=1}^{N/2} \left\{ \begin{array}{c} A_{1,j} \cos(j\Omega t - \varphi_{1,j}) \\ A_{2,j} \cos(j\Omega t - \varphi_{2,j}) \end{array} \right\}. \tag{22}$$

The harmonic amplitudes and phases can be expressed as

$$\begin{array}{l} A_{1,j} = \sqrt{(b_{1,j})^2 + (c_{1,j})^2}, \varphi_{1,j} = \arctan \frac{c_{1,j}}{b_{1,j}}, \\ A_{2,j} = \sqrt{(b_{2,j})^2 + (c_{2,j})^2}, \varphi_{2,j} = \arctan \frac{c_{2,j}}{b_{2,j}}. \end{array} \tag{23}$$

For simplicity, displacement $x(t)$ for period-1 motions is

$$x(t) \approx a_0 + \sum_{j=1}^{N/2} b_j \cos(j\Omega t) + c_j \sin(j\Omega t). \tag{24}$$

Thus,

$$x(t) \approx a_0 + \sum_{j=1}^{N/2} A_j \cos(j\Omega t - \varphi_j) \tag{25}$$

where

$$A_j = \sqrt{(b_j)^2 + (c_j)^2}, \varphi_j = \arctan \frac{c_j}{b_j}. \tag{26}$$

From the discrete nodes of period-1 motions, the corresponding frequency-amplitude characteristics of periodic motions of the van der Pol oscillator can be obtained. For frequency-amplitude curves, the acronym "SN" still represents the saddle node bifurcation. The solid and dashed curves are also used for the stable and unstable periodic motions, respectively.

In Figure 2, global views of harmonic amplitudes varying with excitation frequency for periodic motions in the van der Pol oscillator are presented for $Q_0 =$ 100, 50, 30, 20, 10, 5, 1 and 0.1. Most of period-1 motions in the van der Pol oscillator is symmetric. For symmetric period-1 motions, $a_0 = 0$, $A_{2l} = 0$ but $A_{(2l-1)} \neq 0$ $(l = 1, 2, \ldots)$. The harmonic amplitudes A_1 varying with excitation frequency is presented in Figure 2a for aforementioned different excitation amplitudes. For $Q_0 = 100$,

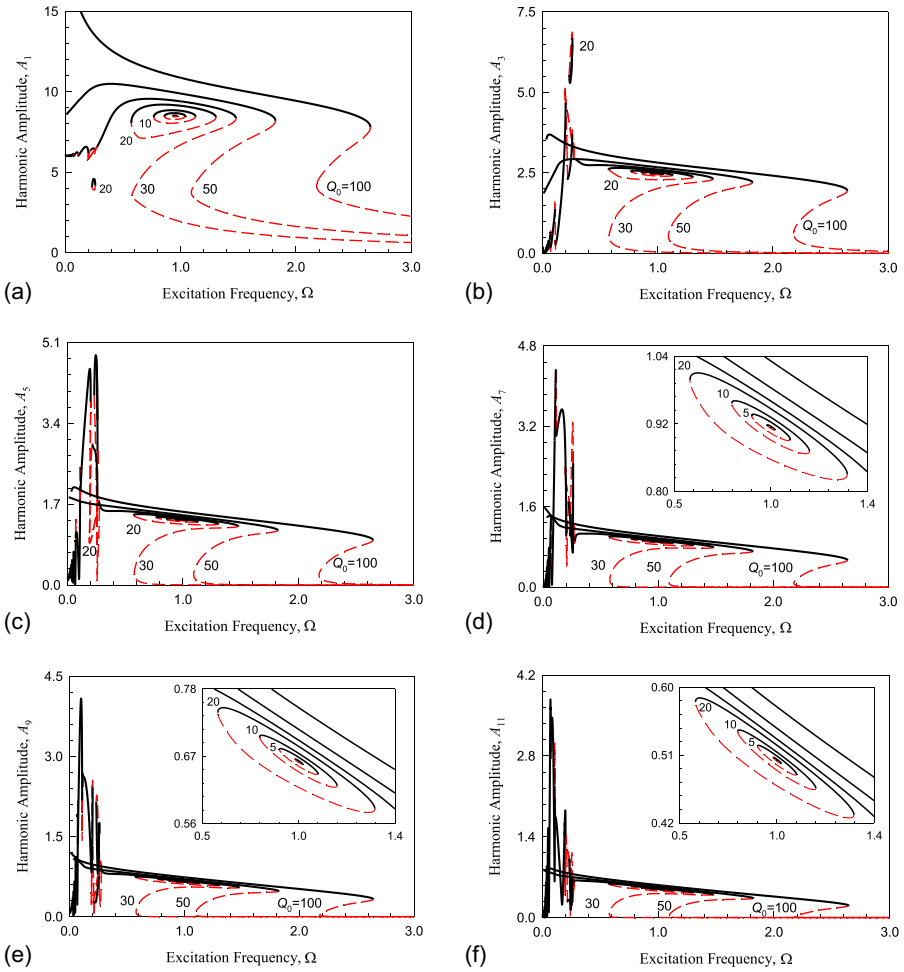

Fig. 2. Frequency-amplitude characteristics of periodic motions ($\Omega \in (0, 3)$). (a)–(f) A_{2k-1} $(k = 1, 2, \ldots, 6)$ $(\alpha_1 = 16,\ \alpha_2 = 1,\ \beta = 5)$ with $Q_0 = 100, 50, 30, 20, 10, 5, 1, 0.1$.

the periodic motion is stable in $\Omega \in (0, 2.645)$ and unstable in $\Omega \in (2.193, 2.645)$ and $(2.193, \infty)$. When the stable period-1 motion becomes unstable, a saddle-node bifurcation occurs, and the jumping phenomenon of such a period-1 motion is caused by such a saddle-node bifurcation. The period-1 motion for $Q_0 = 50$ is stable for $\Omega \in (0, 1.823)$ and unstable for $\Omega \in (1.105, 1.823)$ and $(1.105, \infty)$ with a saddle-node bifurcation of $\Omega = 1.823$. For $Q_0 = 30$, the asymmetric and symmetric period-1 motions exist. For $Q_0 = 20$, the periodic motion exists in the range of $\Omega \in (0.573, 1.306)$. For $Q_0 = 10$, 5, 1 and 0.1, the period-1 motions are in the finite ranges of frequency. As $Q_0 \to 0$, the frequency ranges of the periodic motion approach to a point, which is for limit cycle. For $Q_0 = 10$, the frequency range is in $\Omega \in (0.768, 1.123)$. The frequency ranges of period-1 motions for $Q_0 = 5.0, 1.0,$ and 0.1 are $\Omega \in (0.860, 1.040)$, $\Omega \in (0.933, 0.969)$ and $\Omega \in (0.949, 0.953)$, respectively. The two ends of the frequency ranges are saddle-node bifurcations, and the quantity level of A_1 is $A_1 \sim 10^1$. The harmonic amplitude A_3 varying with excitation frequency is presented in Figure 2b and the third order harmonic amplitude A_3 has the quantity level of $10^0 \sim 10^1$. Similarly, the harmonic amplitudes of A_5, A_7, A_9 and A_{11} are presented in Figures 2c–2f, and the corresponding quantity levels of $10^0 \sim 10^1$.

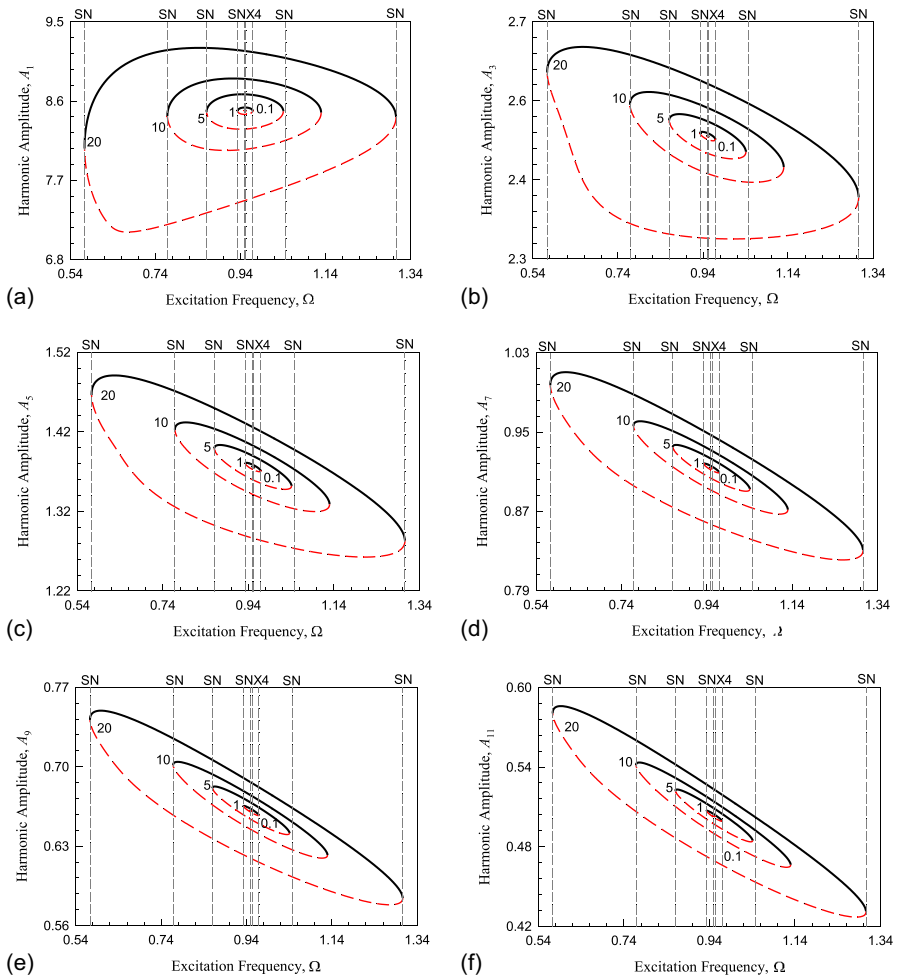

Fig. 3. Frequency-amplitude characteristics of periodic motions ($\Omega \in (0.54, 1.34)$). (a)–(f) $A_{2k-1}(k = 1, 2, \ldots, 6)$ ($\alpha_1 = 16, \quad \alpha_2 = 1, \quad \beta = 5$) with $Q_0 = 20, 10, 5, 1, 0.1$.

For $Q_0 \leq 20$, the harmonic amplitudes of period-1 motions are clopped loops. With harmonic order increase, the closed loops are much closer to the harmonic amplitudes for $Q_0 > 30$. Thus, the first zoomed views of A_{2k-1} $(k = 1, 2, \ldots, 6)$ for $Q_0 \leq 20$ are presented in Figures 3a–3f. The frequency-amplitude characteristics are very clearly presented, and the quantity levels for all of the harmonic amplitude are very close. The second zoomed views of harmonic amplitudes of A_{2k-1} $(k = 1, 2, \ldots, 6)$ for $Q_0 = 30, 50, 100$ are presented in Figures 4a–4f. The frequency-amplitude characteristics of symmetric and asymmetric period-1 motions are clearly presented. To further look into the frequency-amplitude characteristics, the harmonic amplitudes of A_{10k-1} $(k = 2, 3, \ldots, 7)$ are presented in Figures 5 and 6. The corresponding quantity levels of the harmonic amplitudes drop very slowly. Especially, the harmonic amplitudes of A_{10k-1} $(k = 2, 3, \ldots, 7)$ for $Q_0 = 0.1, 1.0, 5.0, 10, 20$ are with quantity levels of $A_{19} < 0.3$, $A_{29} < 0.155$, $A_{39} < 0.09$, $A_{49} < 0.05$, $A_{59} < 0.036$, $A_{69} < 0.024$. Similarly, other higher order harmonic amplitudes can be presented. Because of the slow-fast varying system, the decay rates of harmonic amplitude are very slow with harmonic order. For low excitation frequency, the periodic motions need over hundreds of harmonic terms to be described with a certain accuracy.

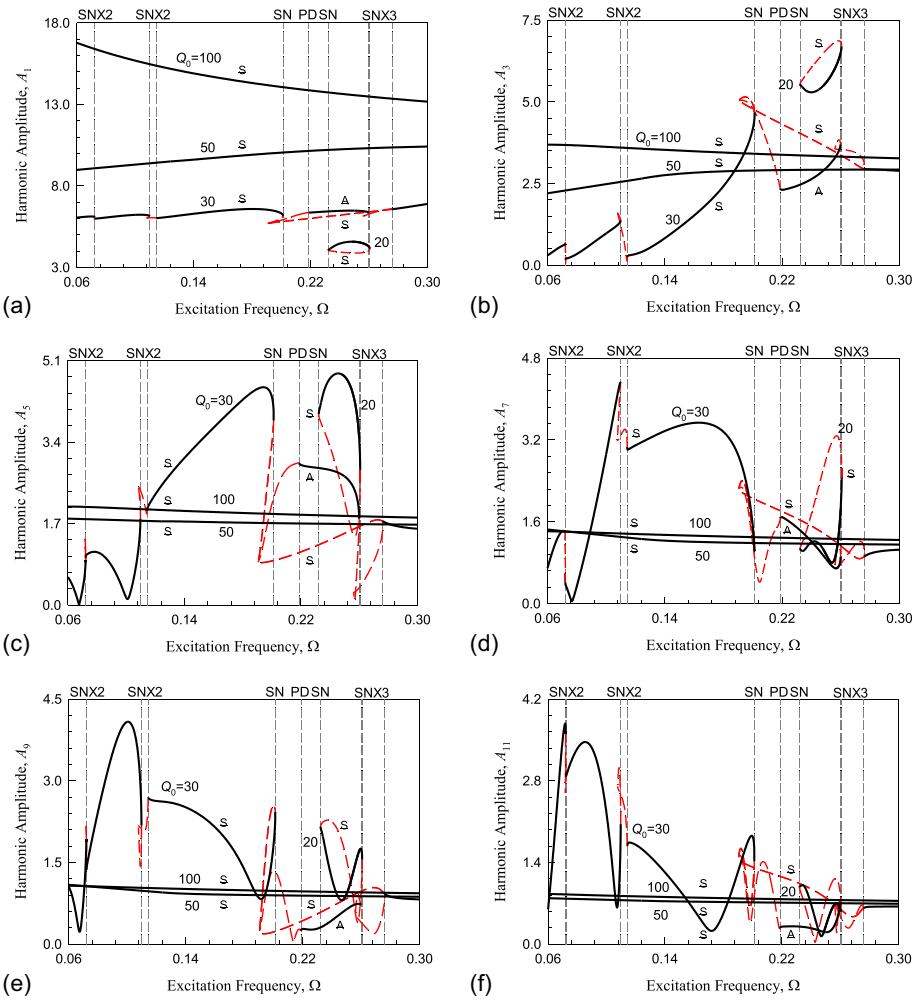

Fig. 4. Frequency-amplitude characteristics of periodic motions $\Omega \in (0.06, 0.30)$. (a)–(f) A_{2k-1} $(k = 1, 2, \ldots, 6)$ $(\alpha_1 = 16, \quad \alpha_2 = 1, \quad \beta = 5)$ with $Q_0 = 100, 50, 30$.

5 Numerical simulations

To observe the complex period-1 motions, numerical solutions of the periodic motions are computed by the midpoint integration method. The initial conditions for numerical simulations are selected from the semi-analytical solutions. The displacements, trajectories, harmonic amplitudes and phases will be presented. The circular symbols and solid curves represent analytical and numerical results. The acronym "I.C." represents initial conditions marked by larger circular symbols.

The numerical simulation for a stable periodic motion is presented in Figure 7 for $Q_0 = 0.1$ and $\Omega = 0.952$. The rest parameters are the same as in equation (17). The initial condition for such illustration is $\mathbf{x}_0 \approx (-5.1354, 2.2129)^{\mathrm{T}}$. In Figure 7a the time-history of displacement is presented, and two slowly varying motions plus two spikes form a periodic motion. The phase trajectory (x, y) of the stable periodic motion is plotted in Figure 7b. The slowly varying zone and fast spike motions are clearly observed, and the motion symmetry is also observed. The harmonic amplitudes of displacement in such a stable periodic motion are presented

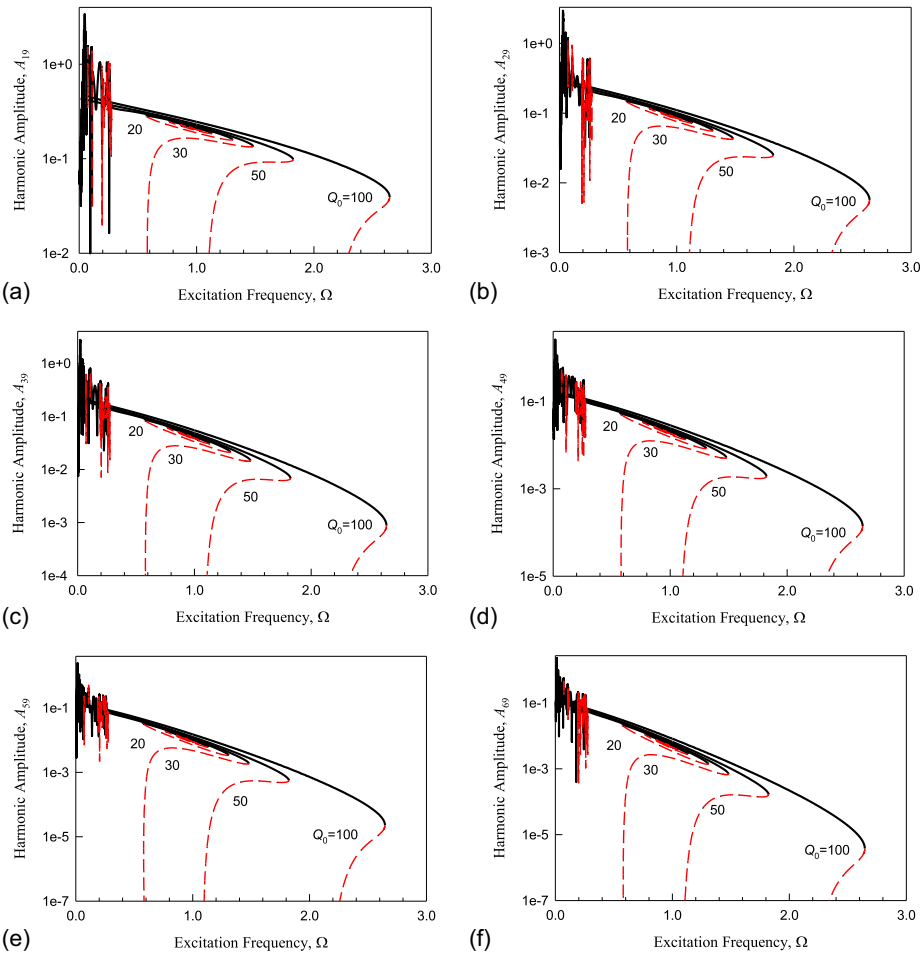

Fig. 5. Frequency-amplitude characteristics of periodic motions ($\Omega \in (0,3)$). (a)–(f) $A_{10k-1}(k=2,3,\ldots,7)$ ($\alpha_1=16,\ \alpha_2=1,\ \beta=5$) with $Q_0=100,50,30,20,10,5,1,0.1$.

in Figure 7c. For the symmetric periodic motion, the constant term is zero. The main harmonic amplitudes are $A_1\approx 8.4913$, $A_3\approx 2.4828$, $A_5\approx 1.3754$, $A_7\approx 0.9134$, $A_9\approx 0.6612$, $A_{11}\approx 0.5031$, $A_{13}\approx 0.3953$, $A_{15}\approx 0.3176$, $A_{17}\approx 0.2594$, $A_{19}\approx 0.2144$, $A_{21}\approx 0.1789$, $A_{23}\approx 0.1504$, $A_{25}\approx 0.1272$, $A_{27}\approx 0.1081$. The other harmonic terms are $A_k\in(10^{-14},10^{-1})$ ($j=29,31,\ldots,499$) with $A_{499}\approx$ 1.91e-14. The harmonic phases are presented in Figure 7d. Such a periodic motion is very close to the limit cycle. Such a period-1 motion needs 255 odd harmonic terms to be described with accuracy of $\varepsilon=10^{-14}$.

In Figure 8, a symmetric periodic motion for $\Omega=0.256$ and $Q_0=30$ is presented with the initial condition of $\mathbf{x}_0\approx(6.1967,-0.0445)^{\mathrm{T}}$. The displacement response of the period-1 motion is presented in Figure 8a. Four pieces of slowly varying motions plus two big spikes and two small spike motions are to form a period-1 motion. The phase trajectory of such a period-1 motion is presented in Figure 8b and two small cycles on the left and right sides exist, which from the small spike motions. The corresponding harmonic amplitude spectrum is presented in Figure 8c. The main harmonic amplitudes are $A_1\approx 6.3674$, $A_3\approx 3.4819$, $A_5\approx 1.5813$, $A_7\approx 1.2193$, $A_9\approx 0.9184$, $A_{11}\approx 0.6813$, $A_{13}\approx 0.6494$, $A_{15}\approx 0.4424$, $A_{17}\approx 0.5008$, $A_{19}\approx 0.3092$,

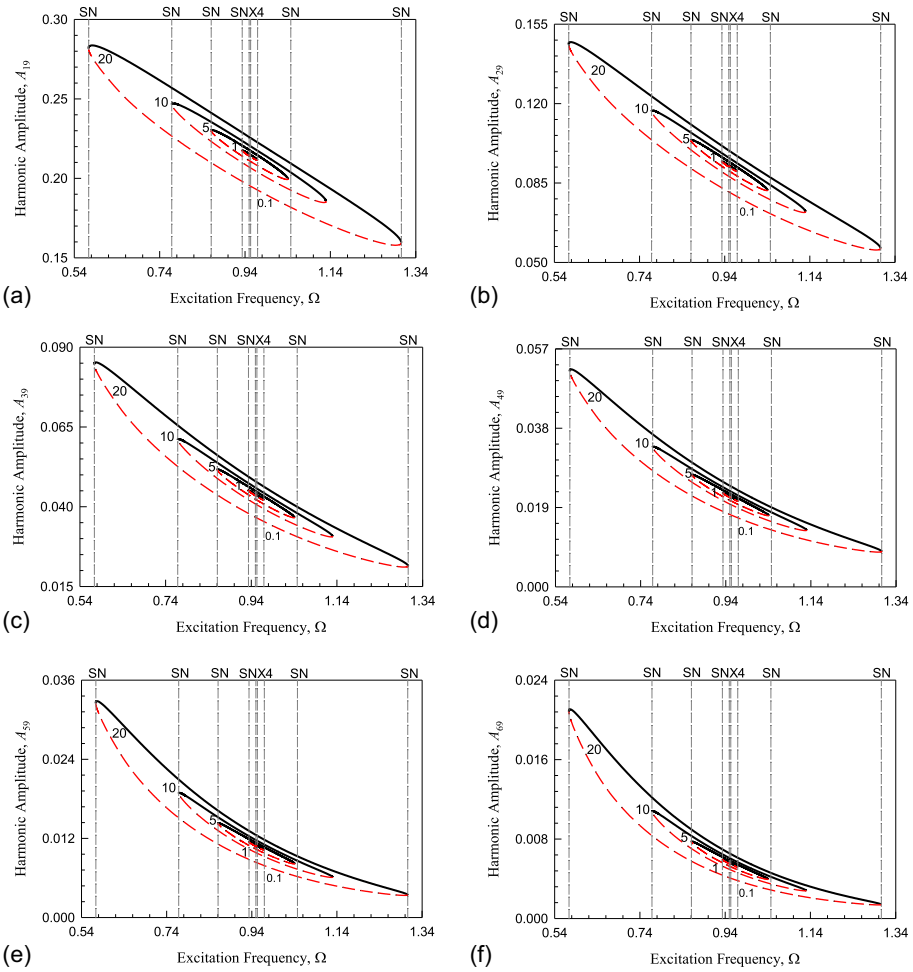

Fig. 6. Frequency-amplitude characteristics of periodic motions ($\Omega \in (0.54, 1.34)$). (a)–(f) $A_{10k-1}(k = 2, 3, \ldots, 7)$ ($\alpha_1 = 16,\ \alpha_2 = 1,\ \beta = 5$) with $Q_0 = 20, 10, 5, 1, 0.1$.

$A_{21} \approx 0.4045,\ A_{23} \approx 0.2261, A_{25} \approx 0.3359, A_{27} \approx 0.1710,\ A_{29} \approx 0.2837,\ A_{31} \approx 0.1335,$ $A_{33} \approx 0.2423,\ A_{35} \approx 0.1077,\ A_{37} \approx 0.2085,\ A_{39} \approx 0.0901,\ A_{41} \approx 0.1803,\ A_{43} \approx 0.0780,$ $A_{45} \approx 0.1564,\ A_{47} \approx 0.0698,\ A_{49} \approx 0.1361,\ A_{51} \approx 0.0639,\ A_{53} \approx 0.1186,\ A_{55} \approx 0.0595,$ $A_{57} \approx 0.1035$. The other harmonic terms are $A_k \in (10^{-12}, 10^{-1})$ $(j = 59, 61, \ldots, 1229)$ with $A_{1229} \approx 4.06\text{e-}12$. The harmonic phases are presented in Figure 8d. Such a period-1 motion needs 615 odd harmonic terms to be described with accuracy of $\varepsilon = 10^{-12}$.

For the van der pol oscillator, it is very difficult to get the asymmetric periodic motion. Herein, a asymmetric periodic motions are illustrated. In Figure 9, an asymmetric periodic motion for $\Omega = 0.24$ and $Q_0 = 30$ is presented with the initial conditions of $\mathbf{x}_0 \approx (5.5534, 0.1549)^{\mathrm{T}}$ (left) and $\mathbf{x}_0 \approx (7.7281, -0.1978)^{\mathrm{T}}$ (right). The displacement responses of the two asymmetric period-1 motions are presented in Figures 9a and 9b. Four pieces of slowly varying motions plus two big spikes and two small spike motions are to form an asymmetric period-1 motion. The phase trajectories of two asymmetric period-1 motion are presented in Figures 9c and 9d. The harmonic amplitudes and phases are presented in Figures 9e and 9f. For the two asymmetric period-1 motions, the two sets of harmonic amplitudes are same except for $a_0^L = -a_0^R \neq 0$ and two sets of harmonic phases satisfy $\varphi_k^L = \mathrm{mod}(\varphi_0^R + (k+1)\pi, 2\pi)$. For asymmetric

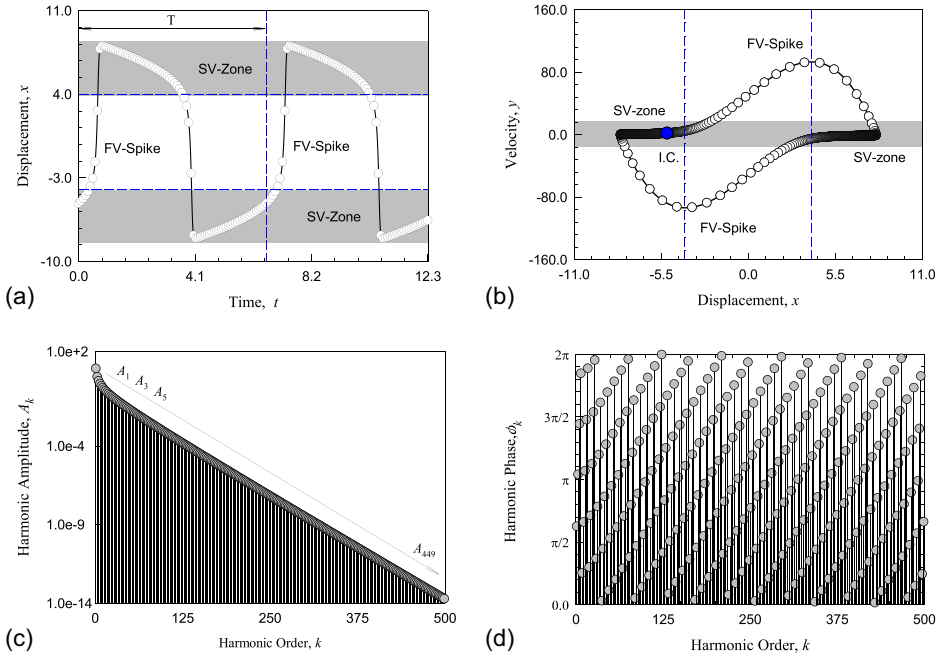

Fig. 7. Symmetric period-1 motion in the van der Pol oscillator at $\Omega = 0.952$ and $Q_0 = 0.1$. (a) Displacement x, (b) velocity y, (c) phase trajectory (x, y), (d) harmonic amplitude A_k, (e) harmonic phase φ_k. Initial conditions $\mathbf{x}_0 \approx (-5.1354, 2.2129)^{\mathrm{T}}$. $(\alpha_1 = 16, \alpha_2 = 1, \beta = 5)$.

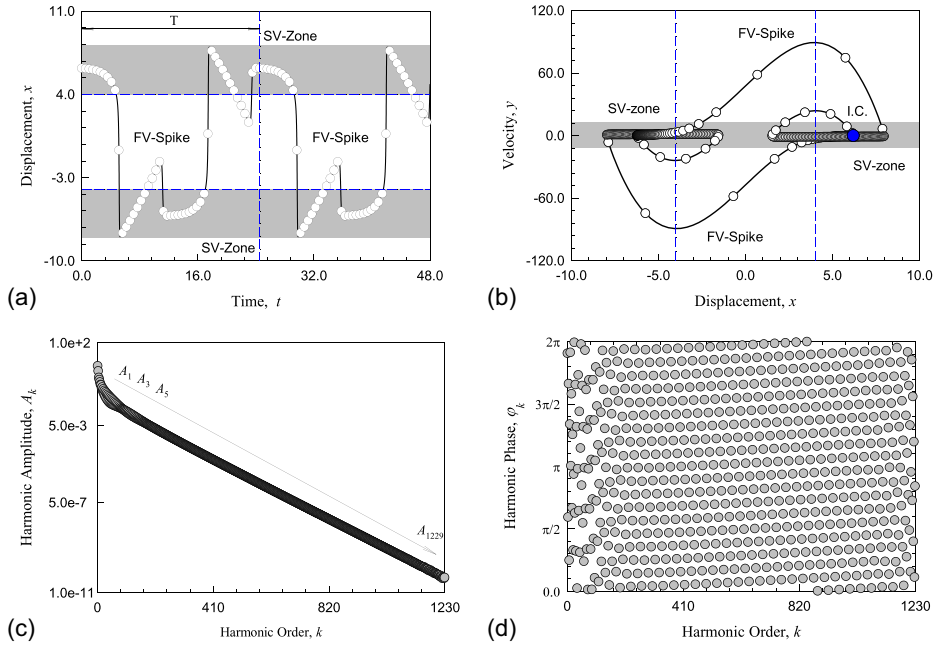

Fig. 8. Symmetric periodic motion in the van der Pol oscillator at $\Omega = 0.256$ and $Q_0 = 30$. (a) Displacement x, (b) phase trajectory (x, y), (c) harmonic amplitude A_k, (d) harmonic phase φ_k. Initial condition: $\mathbf{x}_0 \approx (6.1967, -0.0445)^{\mathrm{T}}$. $(\alpha_1 = 16, \quad \alpha_2 = 1, \quad \beta = 5)$.

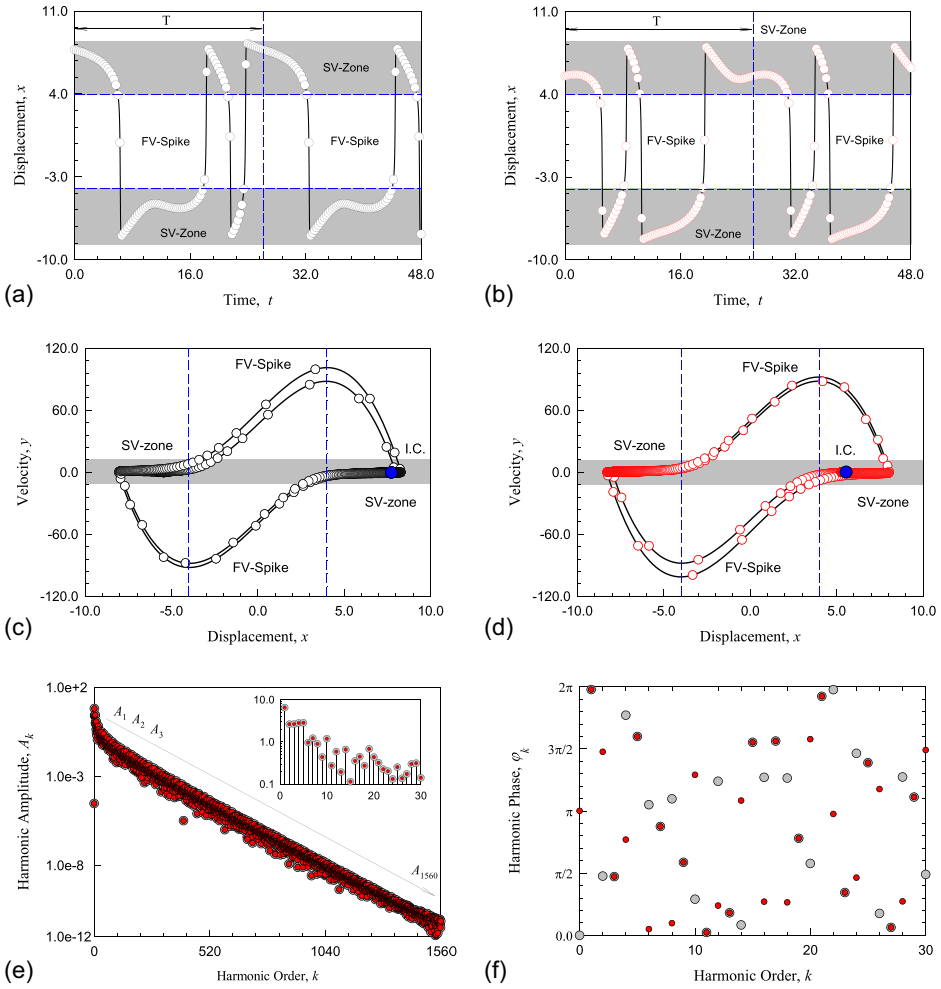

Fig. 9. Asymmetric period-1 motion in the van der Pol oscillator at $\Omega = 0.24$ and $Q_0 = 30$. (a) Displacement x (right), (b) displacement x (left), (c) trajectory (x, y) (right), (d) trajectory (x, y) (left), (e) harmonic amplitude A_k, (f) harmonic phase φ_k. Initial conditions $\mathbf{x}_0 \approx (5.5532, 0.1549)^{\mathrm{T}}$ (left) and $\mathbf{x}_0 \approx (7.7281, -0.1978)^{\mathrm{T}}$ (right). ($\alpha_1 = 16,\ \alpha_2 = 1,\ \beta = 5$).

periodic motions, $A_{2k-1} \neq 0$ and $A_{2k} \neq 0$. $a_0^R = -a_0^L \approx 3.02038\text{e-}5$. The main harmonic amplitudes are $A_1 \approx 6.4723$, $A_2 \approx 2.6252$, $A_3 \approx 2.6350$, $A_4 \approx 2.7940$, $A_5 \approx 2.8185$, $A_6 \approx 0.9610$, $A_7 \approx 1.2164$, $A_8 \approx 0.8915$, $A_9 \approx 0.4359$, $A_{10} \approx 1.1856$. The other harmonic terms are $A_k \in (10^{-12}, 10^0)$ $(j = 11, 12, \ldots, 1560)$ with $A_{1560} \approx 7.30\text{e-}12$. The two asymmetric period-1 motion needs 1560 harmonic terms to be described with accuracy of $\varepsilon = 10^{-12}$.

6 Conclusion

In this paper, nonlinear frequency-amplitude characteristics of periodic motions in a periodically forced van der Pol oscillator were discussed, and the asymmetric period-1 motions were discovered through the semi-analytical method. The period-1 motions of the van der Pol oscillator were determined and the corresponding stability and bifurcation analysis were completed. The nonlinear frequency-amplitude characteristics

of periodic motions were presented from the finite Fourier series analysis. From the frequency-amplitude characteristics, slow-fast motions of periodic motions in the van der Pol oscillator require many harmonic terms to achieve period-1 motions with the certain accuracy, which cannot be determined by the traditional methods (e.g., perturbation methods and series methods). Symmetric and asymmetric period-1 motions were also illustrated numerically and analytically. From the asymmetric period-1 motions, it is possible that the bifurcation trees of period-1 motions to chaos can be obtained in the van der Pol oscillator.

Author contribution statement

Yeyin Xu mainly completed this research. Albert C.J. Luo mainly supervised this research.

References

1. B. van der Pol, Radio Rev. **1**, 754 (1920)
2. W.M.H. Greaves, Proc. R. Soc. London A **103**, 516 (1923)
3. B. van der Pol, J. van der Mark, Nature **120**, 363 (1927)
4. B. Van der Pol, Proc. Inst. Radio Eng. **22**, 1051 (1934)
5. M.L. Cartwright, J.E. Littlewood, J. London Math. Soc. **20**, 180 (1945)
6. M.L. Cartwright, J.E. Littlewood, Ann. Math. **1947**, 472 (1947)
7. J.E. Littlewood, Acta Math. **97**, 267 (1957)
8. N. Levinson, Proc. Natl. Acad. Sci. USA **34**, 13 (1948)
9. N. Levinson, Ann. Math. Second Series **50**, 127 (1949)
10. C.M. Andersen, J.F. Geer, SIAM J. Appl. Math. **42**, 678 (1982)
11. M.B. Dadfar, J.F. Geer, C.M. Andersen, SIAM J. Appl. Math. **44**, 881 (1984)
12. A. Buonomo, SIAM J. Appl. Math. **59**, 156 (1998)
13. A. Buonomo, Int. J. Circuit Theory Appl. **26**, 39 (1998)
14. R.E. Mickens, J. Sound Vib. **245**, 757 (2001)
15. R.E. Mickens, J. Sound Vib. **258**, 199 (2002)
16. S.B. Waluya, W.T. van Horssen, J. Sound Vib. **268**, 209 (2003)
17. I.V. Andrianov, W.T. van Horssen, J. Sound Vib. **295**, 1099 (2006)
18. J.O. Maaita, J. Appl. Nonlinear Dyn. **5**, 193 (2016)
19. S.B. Yamgoué, B. Nana, F.B. Pelap, J. Appl. Nonlinear Dyn. **6**, 17 (2017)
20. B. Shayak, P. Vyas, J. Appl. Nonlinear Dyn. **6**, 57 (2017)
21. S. Rajamani, S. Rajasekar, J. Appl. Nonlinear Dyn. **6**, 121 (2017)
22. A.C.J. Luo, *Continuous Dynamical Systems* (HEP/L&H Scientific, Beijing/Glen Carbon, 2012)
23. A.C.J. Luo, J.Z. Huang, Int. J. Bifurc. Chaos **22**, 1250093 (2012)
24. A.C.J. Luo, J.Z. Huang, J. Appl. Nonlinear Dyn. **1**, 73 (2012)
25. A.C.J. Luo, A.B. Lakeh, Int. J. Dyn. Control **1**, 99 (2013)
26. A.C.J. Luo, A.B. Lakeh, Int. J. Dyn. Control **2**, 474 (2014)
27. A.C.J. Luo, Int. J. Bifurc. Chaos **25**, 1550044 (2015)
28. A.C.J. Luo, *Discretization and Implicit Mapping Dynamics* (HEP/Springer, Beijing/Berlin, Heidelberg, 2015)
29. A.C.J. Luo, Y. Guo, Discontin. Nonlinearity Complex. **4**, 121 (2015)
30. Y. Guo, A.C.J. Luo, Int. J. Dyn. Control **5**, 551 (2016)
31. A.C.J. Luo, S. Xing, Nonlinear Dyn. **85**, 1141 (2016)
32. A.C.J. Luo, S. Xing, Nonlinear Dyn. **88**, 2831 (2017)
33. Y. Xu, A.C.J. Luo, J. Vib. Test. Syst. Dyn. **2**, 119 (2018)
34. Y. Xu, A.C.J. Luo, Int. J. Dyn. Control **7**, 795 (2018)